Comparison of the primary atomization model PAMELA with drop size distributions of an industrial prefilming airblast nozzle

Simon Holz*, Geoffroy Chaussonnet, Sebastian Gepperth, Rainer Koch, Hans-Jörg Bauer
Institut für Thermische Strömungsmaschinen, Karlsruhe Institute of Technology, Germany
*Corresponding author: simon.holz@kit.edu

Abstract
An annular prefilmling airblast nozzle was investigated at ambient conditions with the shadowgraphy technique. The measured volume probability densities and Sauter mean diameters confirm the trends of previous investigations at planar prefilmers, whereby the gas velocity has a major effect on the atomization process compared to the liquid mass flow. Furthermore it could be successfully demonstrated that the Primary Atomization Model for prEfilming airBLast injectors (PAMELA) is able to reproduce the SMD of an annular prefilming airblast nozzle adequately, although it was calibrated with measurements of planar prefilmers.

Introduction
In the near future gas turbines used for aircraft propulsion will have to fulfil more stringent emission regularities. To meet these requirements an understanding of the combustion itself and its influencing parameters is essential. One of these parameters is the fuel injection which is mostly realized by prefilming airblast atomizers.
Prefilming airblast atomizers have a number of advantages including fine atomization, comparatively little change in performance over a wide range of fuel flow rates, and low pressure losses [1]. The spray generation itself can be split up into the following mechanisms: formation of bags and ligaments and their breakup (so called primary breakup) and the subsequent breakup of droplets (so called secondary breakup). The secondary breakup of droplets is widely understood, but the primary atomization is still a topic of active research.
To investigate the atomization process phase Doppler techniques like PDA and direct imaging techniques like shadowgraphy are widely used. Whereas the PDA captures only spherical droplets in a small measurement volume, the shadowgraphy technique is able to analyse liquid structures of any shape over the hole focal plane [2]. Thus the primary breakup, where a huge number of non-spherical droplets occurs, can be investigated better with the shadowgraphy technique than with the PDA.
Whereas planar prefilmers have been investigated by many researchers with PDA [3], Fraunhofer diffraction measurements [4] and shadowgraphy measurements [5, 6, 7], annular prefilming airblast nozzles have been studied only conducting PDA measurements [8, 9, 10]. Thus to the knowledge of the authors no publicised data about the drop size distribution in the primary breakup zone of an annular prefilming airblast nozzles exists.
To design atomizers and combustion chambers CFD simulations are widely used. Although there are several approaches for fully simulating the atomization process like SPH [11] or eDNS [12], these methods are far away from simulating a full combustion chamber with atomization. The reasons are the small scales in time and space which have to be resolved for capturing the atomization process. Thus the CPU and memory consumption for a full combustion chamber prediction would exceed today's computation capacities by far. To overcome this shortage, Euler-Lagrangian CFD simulations with primary atomization models are used. The main purpose of these models is to estimate the spray's initial drop size distribution. So the drop sizes within the region of primary breakup is of major interest. Furthermore these models are based on experimental data and analytical models which use assumptions about the physic of the primary breakup.
In the topic of prefilming airblast atomizers different modelling strategies for the primary breakup have been proposed. In 2010 Gepperth et al. [6] proposed a model which for the first time did not depend on the film thickness but on the boundary layer thickness and other more easily accessible flow quantities. An approach depending on the film thickness was presented by Inamura et al. [4] in 2012. Eckel et al. [13] proposed in 2013 a model which supposes analogously to the model of Inamura et. al [4], longitudinal and transversal waves to build up at the prefilmer, but does not depend on the film thickness. Also in 2013 Gepperth et al. [14] demonstrated by experimental results that the atomizing edge thickness has a strong influence on the SMD, whereas an influence of the mean film thickness was not observed. Therefore Andreini et al. [15] presented in 2014 a modified Senecal model [16] which takes into account the atomizing edge thickness instead of the film thickness. In this context Chaussonnet et al. [17, 18] developed the *Primary Atomization Model for prEfiling airbLAst injectors*, named PAMELA. This model provides a drop size distribution based on the air velocity and the height of the atomizing edge thickness. PAMELA was calibrated with experimental data obtained from planar prefilmers by [19, 5, 14].
Although the same breakup mechanism was observed in a planar and an annular swirled nozzle [20], PAMELA up to now was not compared to experimental results of an annular configuration. To overcome this shortage, the drop size distributions from the annular prefilmling airblast nozzle investigated at ambient conditions by Gepperth et al.

[20] are extracted near the atomizing edge using the shadowgraphy technique [5, 6, 7]. Three different analytical distribution functions are fitted to the measured drop size distributions and compared in terms of sum of squared errors (SSE). Furthermore the measured SMDs are compared to SMDs estimated by PAMELA. In Addition the influences of the air velocity and the considered diameter range on the estimated SMDs are shown.

Experimental setup

Gepperth, Baerow and coworkers [20, 21] investigated the prefilming airblast nozzle discussed in this paper in atmospheric conditions at the Institut für Thermische Strömungsmaschinen (ITS). In this paper, the experimental data of Gepperth is investigated with focus on the droplet size dstribution resulting from the primary breakup process near the atomizing edge.

Prefilming airblast nozzle

The investigated annular prefilming airblast nozzle, depicted in Figure 1, is identical to that investigated by Gepperth et al. [20]. The nozzle consists of a two co-rotating swirlers system, the prefilmer being the separataring wall, as depicted on Figure 1. It is made of perspex for better optical access to the liquid film on the prefilmer. The outer swirler has a shorter exit length, so that the prefilming edge juts out of the nozzle and can be better observed (Figure 1) [21]. The film generation in the nozzle is realized via 42 injection holes on the prefilmer. The diameter of the prefilmer D_{PF} is 15 mm, the distance from the injection holes to the prefilmer's tip L_{PF} is 8 mm and the length of the surface overflown of the gas flow from the primary swirler outlet to prefilmer's tip L_{surf} is about 30 mm. The swirl number S is equal to one for both swirlers. More detailed information about the geometry of the swirl generators can be found in [20].

A substitute fuel is injected on the inner side of the prefilmer and forms a liquid film. Due to momentum exchange with the swirling air flow the liquid film is driven to the atomizing edge and breaks up forming bags, ligaments and droplets downstream the atomizing edge.

The spray generated by a prefilmer is highly influenced by the geometry and the size of the atomizing edge [11, 14]. Therefore an impression of the prefilmer's atomizing edge is presented in Figure 2.

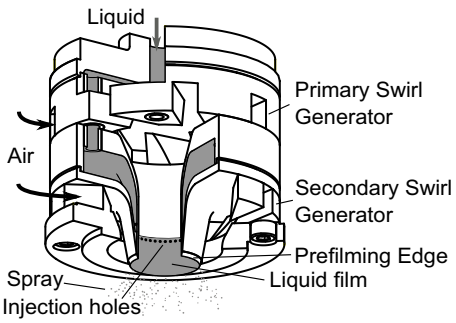

Figure 1. Sketch of nozzle, adapted from [20].

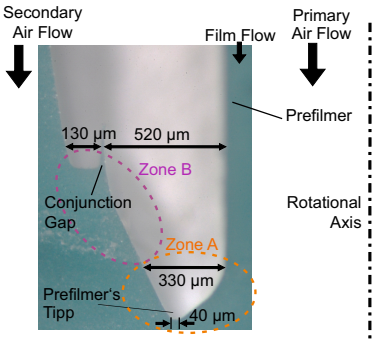

Figure 2. Impression of the prefilmer's atomizing edge.

Operating conditions

The air and liquid mass flow $\dot{m}_{gas}$ and $\dot{m}_{liquid}$ are independently varied over 16 operating points from 10 to 25 g/s and 0.5 to 4.0 g/s, respectively, which corresponds to nominal conditions in industrial gas turbines. The provided air is at ambient pressure and temperature, so that air density ρ_{gas} and viscosity ν_{gas} are 1.21 kg/m^3 and 1.5 10^{-5} m^2/s, respectively. Therefore the bulk velocity u_{bulk} corresponding to $\dot{m}_{gas}$ is 23 to 59 m/s. As substitute fuel Shellsol D70 is used with density ρ_{liquid} = 770 kg/m^3 and surface tension σ = 0.0275 kg/s^2.

Measurement technique

The atomization process was captured using high speed shadowgraphy. The recorded data was further post processed by a Particle and Ligament Tracking Velocimetry (PLTV) algorithm previously developed at the Institut für Thermische Strömungsmaschinen (ITS) by Müller et al. [22, 7]. The drop sizes extracted by the PLTV algorithm are corrected using a calibration plate.

High speed shadowgraphy

The high speed images analysed within this paper have been recorded by Gepperth [20], with a high speed LaVision HighSpeedStar8 camera at a frequency of 50 kHz and a spatial resolution of 27.6 µm per pixel. For each operating point 15.000 images are recorded during a period of 300 ms. The measurement volume is illuminated using a 1 kW halogen spotlight which is mounted opposite of the camera. For a more detailed description of the shadowgraphy

technique the reader is referred to [23].

Particle Ligament Tracking Velocimetry (PLTV)

The particle and ligament tracking velocimetry (PLTV) algorithm developed by Müller et al. [22, 7] is used to extract the droplet's diameter. The algorithm performs the following four steps to extract drop sizes. First, the image brightness and contrast are normalized by two special calibration images called dark image and white image. Second, a contouring algorithm detects closed surface as potential liquid structures. Third, a ellipsoid is fitted to each pixel array. Fourth, the droplet's diameter is estimated under the assumption that the area of the ellipsoid is equivalent to the area of a circle.

Depth of Field and diameter correction

The Depth of Field (DoF) of an optical system is related to the location where the contour of an object is neat. This location is a thick plane perpendicular to the objective axis. The thickness of the plane is called the DoF and determines the size of the object that can be properly resolved by the optical system. The DoF is expressed as [24]:

$$DoF = \frac{2\, f/D\, c\, (\Delta - f)\, \Delta\, f^2}{f^4 - [f/D\, c\, (\Delta - f)]^2} \tag{1}$$

where f and D are the aperture and the diameter of the camera objective, and c is the diagonal of a pixel. In the present study, Eq. 1 leads to DoF = 0.177 mm, which of the order of magnitude of the droplet size contained in the generated spray.

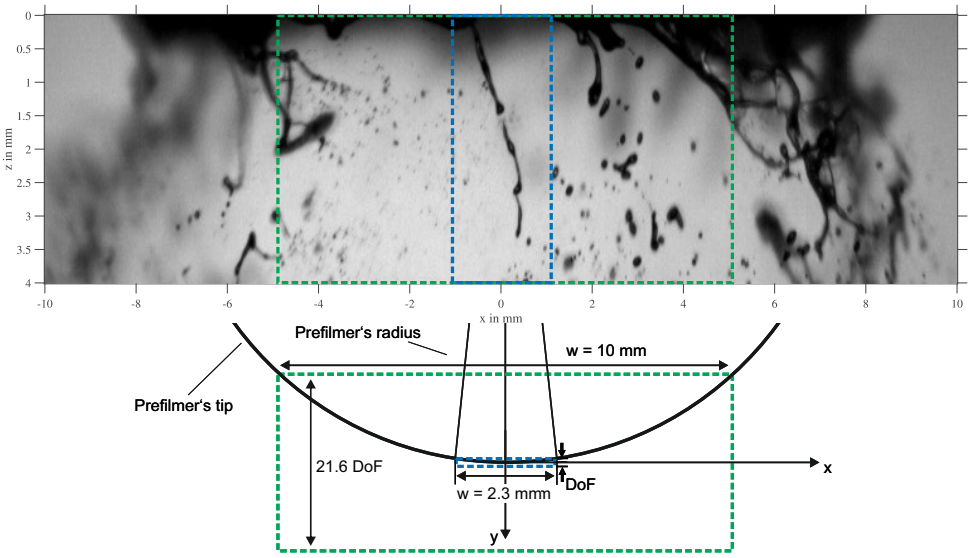

Figure 3. Sketch of the DoF and the horizontal window width

In order to avoid a too large uncertainty on the droplet contour, it would be necessary to account only droplets located in the DoF, which corresponds to a rectangle with a width of 2.3 mm, as depicted in Figure 3. However, this filter would result in a too low number of collected droplets at some operating points, leading to a poor statistical convergence. Therefore, the width of the rectangle was increased to 10 mm, which corresponds to $\approx$ 22 time the DoF. By comparing the resulting SMD with the windows length at the operating points where the statistical convergence was good, it was verified that the second filter does not induce too large distortion (below $\pm$ 10 %).
The diameters extracted by the PLTV algorithm are then corrected with a calibration curve similar to the approach of Müller [23]. The calibration curve was generated by analysing a image of a calibration plate from La Vision with the same PLTV algorithm and settings as used to extract the droplet diameters. Therefore the corrected diameters are in a range of 80 to 1025 µm.

Measurement uncertainty

Gepperth et al. [5] estimated the uncertainty for setting the liquid and gas mass flow at the atmospheric atomization rig below 3.5 %. Müller [23] appreciated the uncertainty of the drop size estimation using a diameter correction below 5 % for diameters within a range of 50 to 600 µm. Due to that, droplets with an uncorrected diameter below 2 px = 55.2 µm are not taken into account. For droplets larger than 600 µm Müller mentioned that the error is unpredictable high because the droplet's shape is getting more and more non-spherical due to high Weber numbers. Therefore

droplets with a uncorrected diameter larger than 1000 µm are neglected. These considerations lead to an over all measurement uncertainty of at least 8.5 % within a diameter range of 50 to 600 µm.

Description of the breakup mode

Snapshots of the breakup process occurring at the atomizing edge are displayed in Figure 4. Herby z = 0 mm corresponds to the position of the atomizing edge. The gas and liquid phases flow from the upper to the lower part of the images. Due to the swirl, a deflection of the liquid to the right is observable. The breakup process shows the same features as in a planar prefilmer [5, 14]: the liquid film accumulates at the tip of the prefilmer and forms a reservoir which is torn apart by the air stream, forming bags and ligaments. From Figure 4, it is observed that the qualitative influence of liquid and gas mass flow rate is the same as observed by Gepperth *et al.* [5]. When the liquid mass flow rate increases, the number of liquid structure (or breakup event) is increased, but the dimension of the ligaments remains slightly the same (Figures 4(a) and 4(b)). When the gas velocity is increased, the size of the ligaments is significantly decreased (Figures 4(b) and 4(d)).

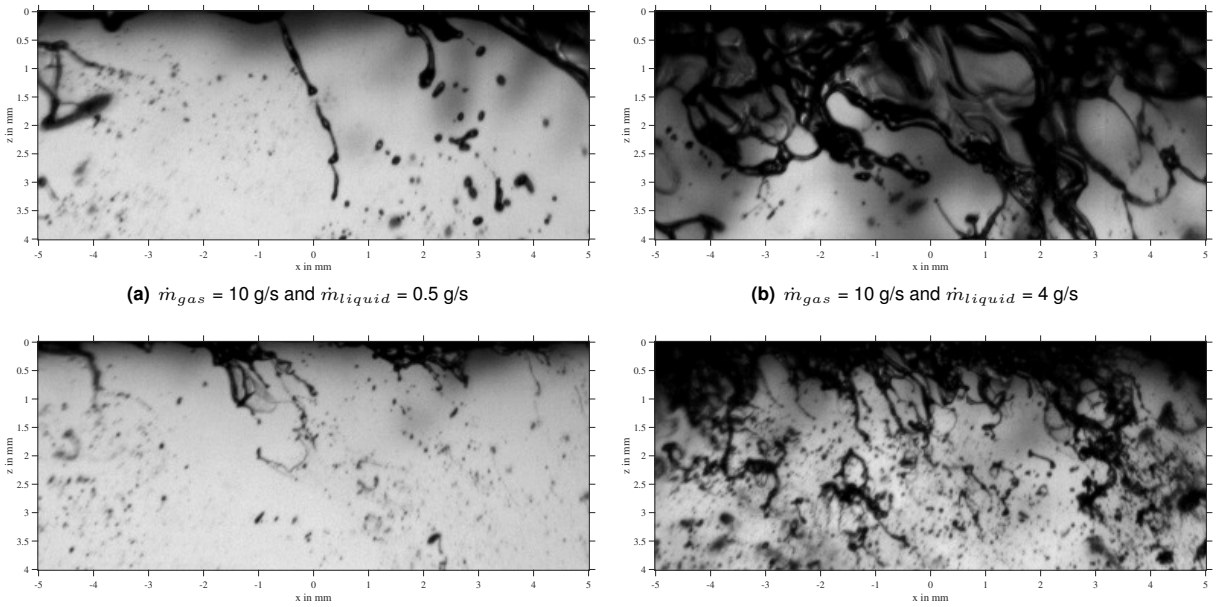

(a) $\dot{m}_{gas}$ = 10 g/s and $\dot{m}_{liquid}$ = 0.5 g/s

(b) $\dot{m}_{gas}$ = 10 g/s and $\dot{m}_{liquid}$ = 4 g/s

(c) $\dot{m}_{gas}$ = 25 g/s and $\dot{m}_{liquid}$ = 0.5 g/s

(d) $\dot{m}_{gas}$ = 25 g/s and $\dot{m}_{liquid}$ = 4 g/s

Figure 4. Snapshot of the breakup process, for different operating points

The PAMELA model

A primary atomization model, named PAMELA for *Primary Atomization Model for prEfiling airbLAst injectors*, was developed [17, 18] to provide instantaneous and local boundary conditions for the simulation of reacting flows inside the combustion chamber. The model does not predict the dynamics of the liquid accumulation and the intermediate ligament, but focuses on the drop size distribution of the spray generated directly downstream the atomizing edge.

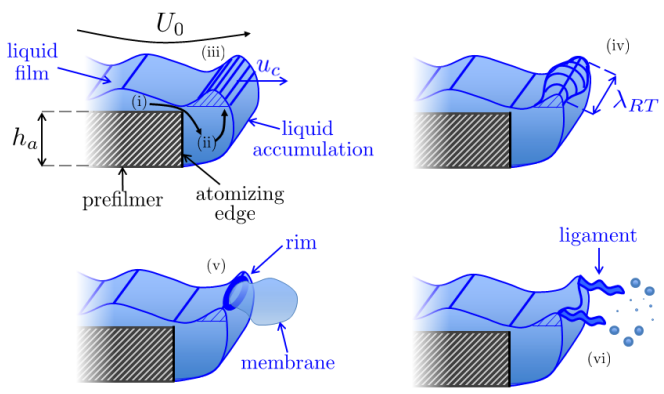

Figure 5. Sketch of the breakup mechanism, adapted from [18].

It is based on experimental observations and proposes the scenario as depicted in Figure 5. The film flow feeds the liquid reservoir (i) which is partly immersed into the high-speed air flow (ii). Due to the high velocity difference, the surface of the liquid reservoir is sheared and strongly accelerated (iii) in the longitudinal direction, leading to a Rayleigh-Taylor instability that develops in the transverse direction (iv). This instability generates crests on the liquid surface that are blown up by the high-speed gas (v), and finally disrupt into bags and ligaments (vi).

It is assumed that the SMD of the generated spray is proportional to the theoretical wave-

length λ_{RT} of the transverse instability, and that the number drop size distribution of the spray follows the Rosin-Rammler function defined by:

$$f_0(d) = q\, m^{-q}\, d^{q-1} \exp\left[-\left(\frac{d}{m}\right)^q\right] \tag{2}$$

where m and q are the *scale* and *shape* parameters, respectively. The former has the dimension of a length and determines the characteristic size of the spray while the latter depicts the width of the central peak, *i.e.* the droplet size dispersion within the spray.
To determine λ_{RT}, it is assumed that the amount of liquid accelerated by the air stream is proportional to the atomizing edge thickness h_a, leading to the expression of $\lambda_{RT}^{h_a}$:

$$\lambda_{RT}^{h_a} \;=\; \frac{2\pi}{r_\rho\, u_g^*}\sqrt{\frac{6\; C_1\; h_a\; \sigma}{\rho_g}} \text{ with } r_\rho = \frac{\sqrt{\rho_l}}{\sqrt{\rho_l}+\sqrt{\rho_g}} \tag{3}$$

where C_1 is a constant, and the term u_g^* represents the mean gas velocity at the location where the breakup occurs. Assuming that the SMD of the spray is proportional to $\lambda_{RT}^{h_a}$ and expressing the SMD of a spray following a Rosin-Rammler distribution, one can link the scale parameter m to the transverse wavelength by:

$$m \;=\; C_2\, \lambda_{RT}^{h_a}\, \frac{\Gamma(2/q+1)}{\Gamma(3/q+1)} \tag{4}$$

where C_2 and Γ are a constant and the gamma function, respectively. The shape parameter q controls the width of the peak and is assumed to depend on the aerodynamic effects and the atomizing edge thickness only. It is thus expressed as a function of the aerodynamics Weber number $\mathrm{We}_\delta = \rho_g \delta u_g^2/\sigma$ where δ is the thickness of the boundary layer on the prefilmer prior to the atomizing edge. It yields:

$$q(\mathrm{We}_\delta, h_a) \;=\; \frac{C_3}{\sqrt{\mathrm{We}_\delta}} + \left(\frac{h_a}{C_4}\right)^2 + C_5 \tag{5}$$

where C_3 to C_5 are the last constants of the model. The overview of the model is depicted in Fig. 6 and highlights the main steps to obtain the spray drop size distribution. The constants C_1 to C_5 were determined using

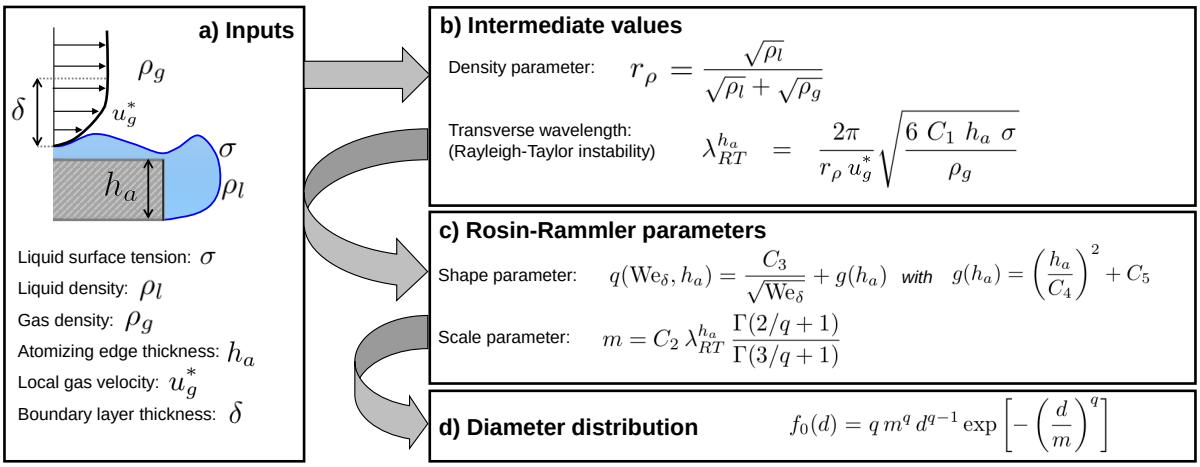

Figure 6. Overview of the PAMELA model

the experimental results from [19, 5, 14]. C_1 was found by comparing the transverse wavelength of water and ethyl-alcohol films atomized by air flowing at a velocity between 20 and 90 m/s. C_2 was set by comparing the SMD of the spray just directly downstream the atomizing edge with Eq. 3. Constants C_3 to C_5 were derived by matching the experimental drop size distribution with a Rosin-Rammler function and fitting the shape q parameter. For C_2 to C_5, the investigated liquids were Shellsol D70 and a volume mixture of 50% Propanediol and 50% of water.

The PAMELA model present two type of use, depending on the type of input parameters listed in Fig. 6. The first type of use is to embeed the model into a CFD code, to provide local and instantaneous spray boundary conditions. More details about the local mode can be found in [18]. Therefore the model relies on *local* input provided by the flow solver. The second type of use is a *global* mode where the input values are determined from global

boundary conditions. In this study, the model is used in global mode, and the determination of the global input parameters is discussed in the following.
The first set of inputs are the physical properties of the gas and the liquid (ρ_{liquid}, ρ_{gas} and σ), and they are easily determined from the operating conditions. The second set of inputs are the geometrical features of the nozzle, *i.e.* the thickness of the atomizing edge h_a and the total length of the prefilmer L_{surf}. Due to a complex shape of the prefilmer lip (Figure 2), the determination of h_a is not obvious and therefore it is necessary to clarify its purpose in the model: it is used to size the amount of liquid accelerated by the high speed air flow, and, in a given range, it is equal to the thickness of the liquid accumulation. At first, it is expected from Figure 2 that the liquid accumulation covers the atomizing edge until the tip of the prefilmer, leading to an atomizing edge thickness of $\approx$ 300 µm. However, SPH (Smooth Particle Hydrodynamics) numerical simulations of a similar geometry [25] showed that the liquid goes beyond the tip and spills on the other side. Therefore the size of the atomizing edge might be $\approx$ 330 µm. In addition, this spilling effect might be enhanced by the conjunction gap on the secondary airflow side depicted in Fig. 2. This gap can be seen as a tiny backward facing step which might induce a recirculation zone and would allow the liquid to be trapped in this zone. In these conditions, the atomizing edge thickness is taken to 650 µm. The total lenght of the prefilmer L_{surf} is used to determine the thickness of the boundary layer δ and therefore is does not correspond to the prefilming length, but the total length of the separator, equal to 30 mm. The boundary layer is expressed as in [5] by:

$$\delta = 0.16\,\frac{L_{surf}}{\mathrm{Re}^{1/7}} \quad \text{with} \quad \mathrm{Re} = \frac{u_{gas}\,L_{surf}}{\nu_{gas}} \tag{6}$$

Finally, the local velocity u_g^* is the most sensitive input parameter due to its larger exponent magnitude (-1) in Eq. 3. In the planar prefilmer configuration, the bulk velocity is parallel to the local velocity seen by the liquid accumulation, and it was observed by [18] that the local velocity magnitude corresponds to 70% of the bulk velocity:

$$u_g^* = 0.7\,u_{bulk} \tag{7}$$

Equation 7 was determined by the observation of the mean turbulent velocity profile downstream a backward facing, and it is assumed valid for any type of configuration where a turbulent boundary layer is established on the prefilmer. Therefore Equation 7 is a part of the model and it is not modified here. However, the present configuration is an annular swirling flow, implying that the bulk velocity is not representative of the mean velocity magnitude at the tip of the prefilmer. As the swirl number is equal to one, the azimuthal component is equal to the axial component, so that the mean velocity magnitude, *i.e.* the global velocity u_{gas} to be input to the model, should be equal to $\sqrt{2}\,u_{gas}$. Additionally, due to centrifugal effects, the axial velocity profile across the nozzle is also modified in comparison to the planar configuration, as it shows a larger value close to the inner side of the prefilmer, where the liquid accumulation is fragmented. The SPH simulation of a similar nozzle [25] showed a velocity magnitude in the vicinity of the prefilmer $\approx$ 50% larger that the mean axial velocity. Therefore, the velocity to input to the model should multiplied by $\approx$ 1.5.
The superposition of the two above-mentioned effects leads to an input velocity:

$$u_{gas} \approx 2\,u_{bulk} \quad \Leftrightarrow \quad u_g^* \approx 1.4\,u_{bulk} \tag{8}$$

In the section dedicated to the results analysis, the importance of the swirl effect in the input velocity is illustrated by setting it to u_{bulk} (no swirl effects accounted) or to 2 u_{bulk} (swirl effects accounted).

Results and Discussion
First measured volume probability densities (vpds) and SMDs will be shown. Second three analytical distribution functions will be tested to fit the measured vpds. Third the measurements are compared to PAMELA in terms of volume pdf and SMD.

Measured drop size distributions
The volume probability densities for four operating points are depicted in Figure 7. An increase in gas mass flow or velocity shifts the peak of the volume probability density from around 200 µm to about 100 µm. Decreasing liquid mass flows seem to slightly support this trend. This behaviour coincidences with the observations of Gepperth et al. [5] who described that the gas velocity has a major effect on the atomization process whereas the liquid mass flow has only a minor effect.

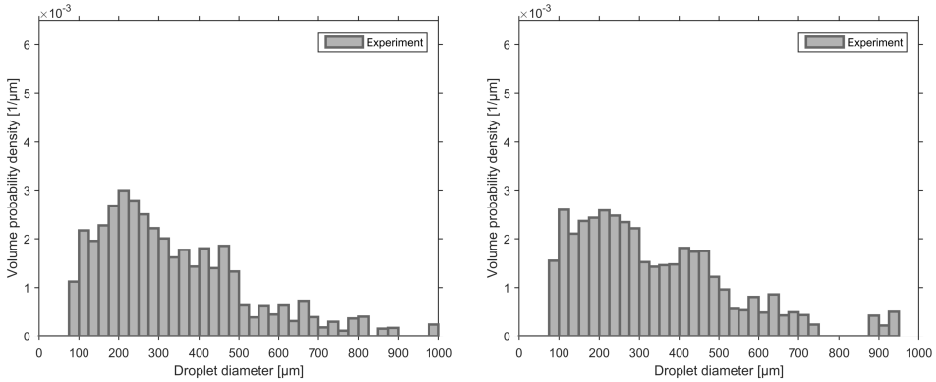

(a) $\dot{m}_{air} = 10.0\ g/s$ and $\dot{m}_{liquid} = 0.5\ g/s$

(b) $\dot{m}_{air} = 10.0\ g/s$ and $\dot{m}_{liquid} = 4.0\ g/s$

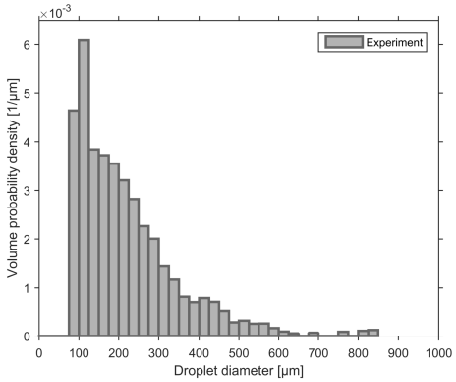

(c) $\dot{m}_{air} = 25.0\ g/s$ and $\dot{m}_{liquid} = 0.5\ g/s$

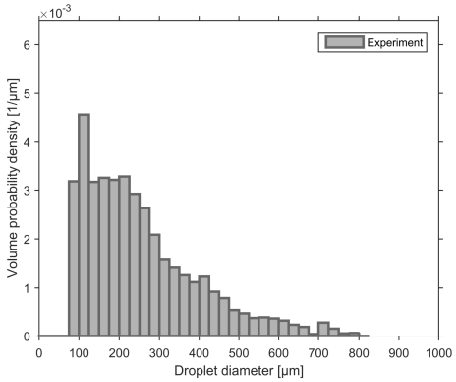

(d) $\dot{m}_{air} = 25.0\ g/s$ and $\dot{m}_{liquid} = 4.0\ g/s$

Figure 7. Volume probability densities of selected operating points.

In Figure 8 the Sauter Mean Diameter (SMD) over the air mass flow is depicted for different fuel mass flows. As expected, the SMD decreases with increasing gas velocity. At medium and high air mass flows (15, 20, 25 g/s) only

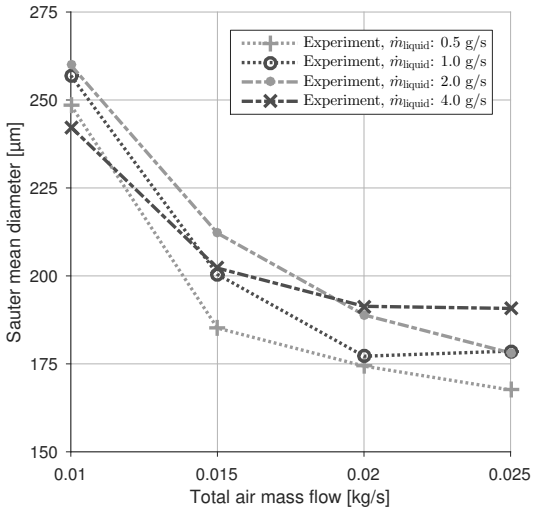

Figure 8. Influence of air and liquid mass flow on the SMD extracted from the Experiment.

a slight decrease in SMD can be observed. This behaviour might be explained by the low resolution of the high speed images: the measured diameters are in a range of about 80 to 1025 µm after the correction, so that droplets smaller than 80 µm are not captured. As droplet diameters decrease with increasing gas velocity, it means that more smaller droplets are filtered at large velocities, leading to an overestimated SMD. For the different liquid mass flows only a slight trend to higher SMDs with increasing liquid mass flow can be noticed at high gas mass flows.

Fit of several distributions to the measured drop size distributions

One of the most relevant distribution in the context of spray generation is the Rosin-Rammler distribution, originally established as cumulative volume distribution function $F_{3,RR}(D)$ for powders by Rosin and Rammler [26]. A derivation of $F_{3,RR}(D)$ leads to the volume probability density function (vpdf) $f_{3,RR}(D)$.

$$F_{3,RR}(D) = 1 - e^{-\left(\frac{D}{m}\right)^q} \quad \Leftrightarrow \quad f_{3,RR}(D) = D^{q-1}\, m^{-q}\, q\, e^{-\left(\frac{D}{m}\right)^q} \tag{9}$$

Chaussonnet *et al.* [17, 18] used Rosin's and Rammler's definition (Equation 9) to describe the cumulative number distribution function $F_0(D)$, leading to the volume PDF:

$$f_{3,ChRR}(D) = D^{q+2}\, m^{-q}\, q\, e^{-\left(\frac{D}{m}\right)^q} \tag{10}$$

where the exponent of D changes from q-1 to q+2.
Rizk and Lefebvre modified Rosin's and Rammler's definition (Eq. 9) to obtain a better fit for large droplets [26]:

$$F_{3,modRR}(D) = 1 - e^{-\left(\frac{\ln(D)}{\ln(m)}\right)^q} \quad \Leftrightarrow \quad f_{3,modRR}(D) = D^{-1}\, \ln(D)^{q-1}\, \ln(m)^{-q}\, q\, e^{-\left(\frac{\ln(D)}{\ln(m)}\right)^q} \tag{11}$$

To quantify the concurrence between the measured volume probability densities $q_3(D)$ and the volume probability density functions $f_3(D)$ the sum of squared errors (SSE) is used as goodness-of-fit criteria.

$$SSE = \sum_{i=1}^{n} \left(q_3(D) - f_3(D)\right)^2 \tag{12}$$

In terms of SSE at low to medium liquid mass flows (0.5 to 2.0 g/s) Chaussonnet's Rosin-Rammler vpdf $f_{3,ChRR}$ (Eq. 10) is slightly better than the modified Rosin-Rammler vpdf $f_{3,modRR}$ (Eq. 11). At high liquid mass flows (4.0 g/s) the modified Rosin-Rammler vpdf $f_{3,modRR}$ shows a slightly better match with the measured vpd q_3. The Rosin-Rammler vpdf $f_{3,RR}$ (Eq. 11) has the worst concurrence of all three vpdfs. Nevertheless all volume probability density functions follow the measured volume probability densities quite well, as depicted in Figure 9.

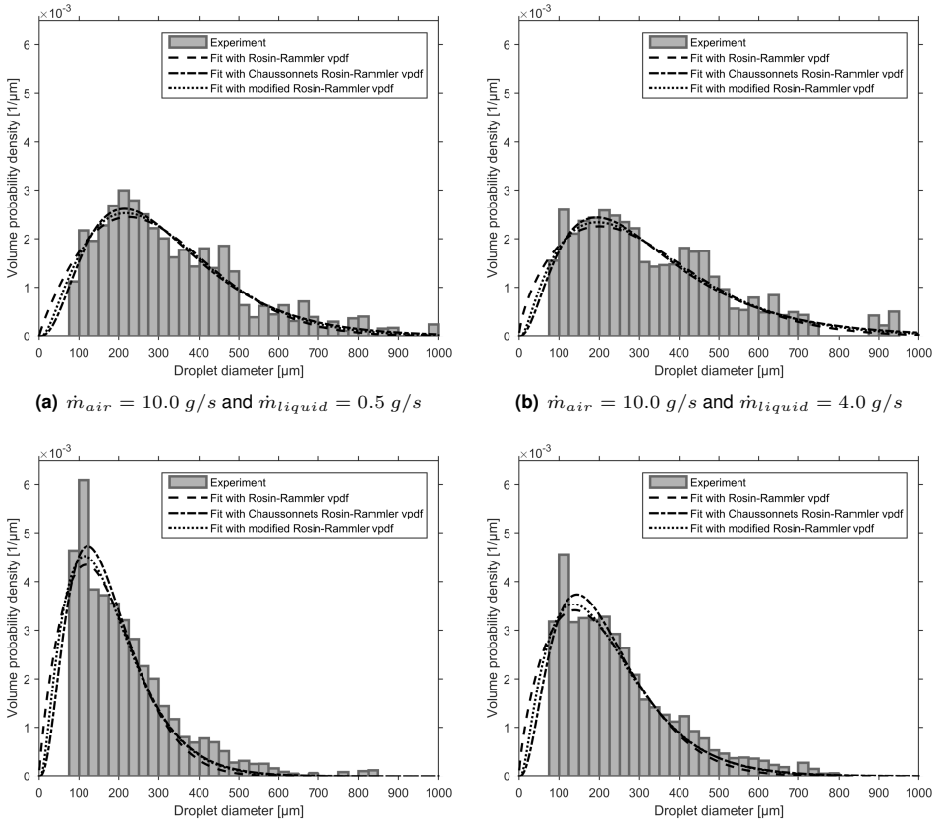

(a) $\dot{m}_{air} = 10.0\ g/s$ and $\dot{m}_{liquid} = 0.5\ g/s$ **(b)** $\dot{m}_{air} = 10.0\ g/s$ and $\dot{m}_{liquid} = 4.0\ g/s$

(c) $\dot{m}_{air} = 25.0\ g/s$ and $\dot{m}_{liquid} = 0.5\ g/s$ **(d)** $\dot{m}_{air} = 25.0\ g/s$ and $\dot{m}_{liquid} = 4.0\ g/s$

Figure 9. Volume probability densities and fits with analytical distributions for selected operating points.

Comparison of the PAMELA model to the measured drop size distributions

The main parameters of the PAMELA model (Figure 6) are the thickness of the atomizing edge h_a and the velocity of the gaseous phase u_{gas}. These two parameters are varied as documented in Table 1. As discussed above, the effects of swirl and centrifugal force have to be taken into account (set 2) and compared to a situation with no swirl nor centrifugal effect (set 1). Each effect is assumed to scale with $\sqrt{2}\ u_{bulk}$.

Table 1. Different sets of PAMELA

set no	h_a [µm]	u_{gas}
1	650	u_{bulk}
2	650	$2\ u_{bulk}$

The volume pdfs estimated by PAMELA are depicted for two different configurations (sets 1 and 2) in Figure 10. For comparison, the measured volume probability density q_3 and the fit with Chaussonnet's Rosin-Rammler vpdf $f_{3,ChRR}$ are also shown.

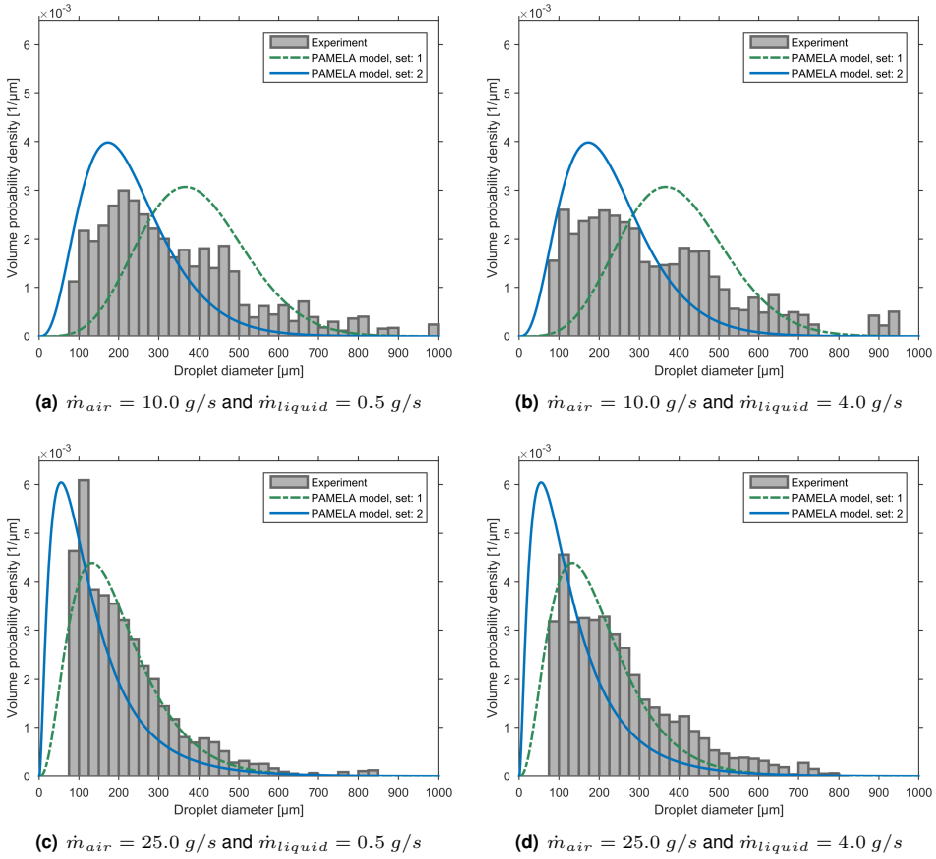

(a) $\dot{m}_{air} = 10.0\ g/s$ and $\dot{m}_{liquid} = 0.5\ g/s$

(b) $\dot{m}_{air} = 10.0\ g/s$ and $\dot{m}_{liquid} = 4.0\ g/s$

(c) $\dot{m}_{air} = 25.0\ g/s$ and $\dot{m}_{liquid} = 0.5\ g/s$

(d) $\dot{m}_{air} = 25.0\ g/s$ and $\dot{m}_{liquid} = 4.0\ g/s$

Figure 10. Volume probability densities, fit with Chaussonnet's Rosin-Rammler and volume pdfs of the PAMELA model for selected operating points.

The increase in atomizing edge thickness h_a and gas velocity shifts the peaks of the vpdf estimated by PAMELA to smaller diameters and for PAMELA set 2 and high gas mass flows even below the lower limit of the spatial resolution of 80 µm. So the vpd of small to medium droplets is highly overestimated by the model. Furthermore droplets large than 500 µm are not taken into account by the model's vpdfs. Compared to Figure 4 spherical droplets with a diameter in the order of 500 µm are quite unreasonable. Most of the structures with a size in that order of magnitude seem to be stretched and therefore non-spherical. This might lead to a significant overestimation of large droplet's volume.

The Sauter mean diameters (SMDs) measured with the shadowgraphy technique and the SMDs estimated by PAMELA sets 1 and 2 are depicted in Figures 11 over the total air mass flow and for different fuel mass flows. The SMDs of PAMELA are determined from a vpdf which ranges from 0 to infinity. In contrast, the measured vpd has

a much smaller diameter range. Therefore in Figure 12 the SMDs for PAMELA set 2 are depicted for a diameter range from 0 to infinity (set 2) and a diameter range from minimal to maximal measured diameter (set 2, SMD cut).

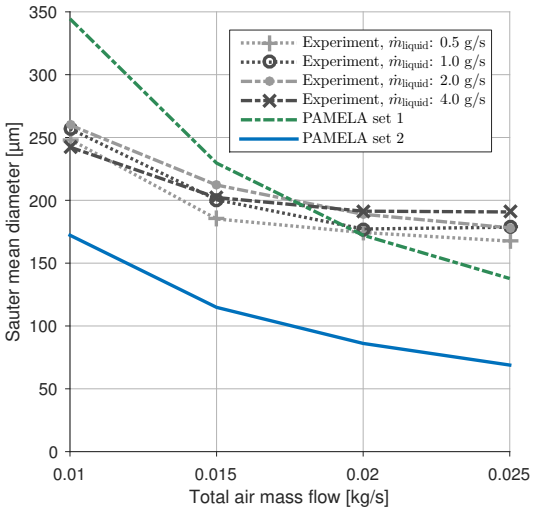

Figure 11. Comparison of the measured SMDs with the SMDs estimated by PAMELA sets 1 and 2

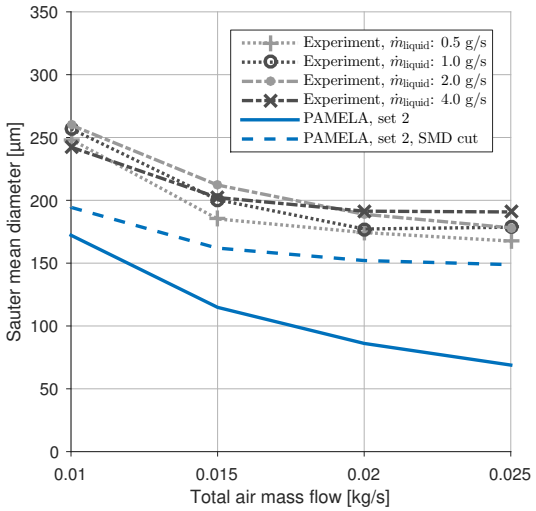

Figure 12. Influence of the reduced diameter range on the SMD estimated by PAMELA sets 2

For parameter set 1 the SMD is overestimated for a low gas velocity and matches satisfactorily at medium to high gas velocities compared to the measurements. With parameter set 2 the estimated SMDs are significantly smaller than the measured SMDs. The over all trend is satisfactorily captured by both sets of the model. However the model shows a substantial steeper decrease in SMD with increasing gas velocity than the measurements.
The significant deviations between the measurements and the model (set 2) may can be explained with the following effects. First, the experimental settings of the measurements used to calibrate PAMELA and the measurements presented in this paper are different. Whereas the model was calibrated using measurements of a planar prefilmer with a defined sharp atomizing edge, in this case an annular nozzle with a curved geometry at the tip and a swirl flow is explored. As shown in Figure 10 this has a tremendous effect on the vpdf estimated by the model.
Second a lot of small droplets might be missed due to the low spatial resolution of the high speed images. May leading to an overestimation in SMD for high gas velocities where significantly more small droplets occur as compared to low gas velocities. This is hypothesis is supported by the trend of set 2, SMD cut in Figure 12 which is in significantly better coincidence with the measurements than set 2. Third Gepperth et al. [20] observed in the annular configuration qualitatively the same breakup mechanism as in the planar configuration. Therefore the presented results seem to be reasonable and reliable.

Summary and Conclusions

The spray near the atomizing edge of an annular prefilmling airblast nozzle was investigated at ambient conditions with the shadowgraphy technique. Three different analytical distributions were fitted to the measured volume probability densities and compared in terms of sum of squared errors (SSE). Furthermore the measured SMDs were compared to SMDs estimated by PAMELA. Finally the influences of the air velocity and the considered diameter range on the estimated SMDs were shown.
The measured volume probability densities and SMDs confirm the trends of previous investigations at planar prefilmers, whereby the gas velocity has a major effect on the atomization process compared to the liquid mass flow. At medium and high air mass flows only a slight decrease in SMD was be observed, might due to the lower measurement limit of 80 µ m in diameter. All three analytical distributions follow the measured volume probability densities quite well. The SMDs estimated by PAMELA show satisfactory coincidence with the measurements when swirl and centrifugal force as well as the diameter ranges of the measurements are taken into account.
It could be successfully demonstrated that the Primary Atomization Model for prEfilming airBLast injectors (PAMELA) is able to reproduce the SMD of an annular prefilming airblast nozzle adequately, although it was calibrated with measurements of planar prefilmers.

Acknowledgements

The research leading to these results has received funding from the European Union's Seventh Framework Programme (FP7/2007-2013) for the Clean Sky Joint Technology Initiative under project DREAMCODE grant n°620143. The authors gratefully acknowledge the work of Lukas Hagmanns during his diploma thesis at the ITS. Furthermore the authors thank Enrico Bärow, Thilo Dauch and Christian Lieber for the fruitful discussions on the topic.

Nomenclature

Abbreviations

DoF	depth of field
eDNS	embedded direct numercial simulation
ITS	Institut für Thermische Strömungsmaschinen english: Institute of Thermal Turbomachines
npd	number probability density
npdf	number probability density function
pdf	probability density function
PAMELA	Primary Atomization Model for prEfiling airbLAst injectors
PDA	Phase Doppler Anemometry
PLTV	particle and ligament tracking velocimetry
SMD	Sauter mean diameter
SPH	smoothed particle hydrodynamics
SSE	sum of squared errors
vpd	volume probability density
vpdf	volume probability density function

Latin Symbols

c	pixel diagonal on CCD-chip [µm]
DoF	depth of field [mm]
D	droplet diameter [µm]
D_{PF}	diameter of the prefilmer [mm]
f/D	aperture to diameter []
f	focal length [mm]
f_0	number probability density function [1/ µm]
f_3	volume probability density function [1/ µm]
F_3	cumulative volume distribution function [1/ µm]
h_a	atomizing edge thickness [µm]
L_{PF}	length of the prefilmer [mm]
L_{surf}	length of the surface overflown by the gas flow [mm]
m	scale factor [µm]
$\dot{m}$	mass flow [kg/s]
q	shape factor []
q_3	measured volume probability density [1/ µm]
S	swirl number []
SSE	sum of squared errors [(µm)^2]
w	horizontal window width [mm]
x	horizontal coordinate [mm]
y	horizontal coordinate [mm]
z	vertical coordinate [mm]

Greek Symbols

Δ	object's distance to camera [mm]
ν	viscosity [m^2/s]
ρ	density [kg/m^3]
σ	surface tension [kg/s^2]

Subscripts

$_0$	number
$_3$	volume
$_{bulk}$	bulk
$_{gas}$	gaseous phase
$_{ChRR}$	Chaussonnet's Rosin-Rammler distribution
$_{liquid}$	liquid phase
$_{modRR}$	modified Rosin-Rammler distribution
$_{PF}$	prefilmer
$_{RR}$	Rosin-Rammler distribution

References

[1] Lefebvre, A. H., *Atomization and Sprays*, 10:251–276 (2000).

[2] Tropea, C., *Annual Review of Fluid Mechanics*, 43:399–426 (2011).

[3] Bhayaraju, U. and Hassa, C., *ICLASS-2006, Kyoto, Japan* (2006).

[4] Inamura, T.; Shirota, M.; Tsushima, M.; Kato, M.; Hamajima, S. and Sato, A., *ICLASS, 12th Triennial International Annual Conference on Liquid Atomization and Spray Systems, Heidelberg, Germany*, Heidelberg, Germany (2012).

[5] Gepperth, S.; Müller, A.; Koch, R. and Bauer, H.-J., Heidelberg, Germany (2012).

[6] Gepperth, S.; Guildenbecher, D.; Koch, R. and Bauer, H.-J., *ILASS Europe, 23rd Annual Conference on Liquid Atomization and Spray Systems, Brno, Czech Republic*, Brno, Czech Rep. (2010).

[7] Müller, A.; Koch, R.; Bauer, H.-J.; Hehle, M. and Schäfer, O., *Proceedings of ASME Turbo Expo 2006: Power for Land, Sea and Air, Barcelona, Spain*, GT2006-90432, Barcelona, Spain (2006).

[8] Schober, P.; Meier, R.; Schäfer, O. and Wittig, S., *International Symposium on Visualization and Imaging in Transport Phenomena (Annals of the New York Academy of Sciences)*, 972:277 – 284 (2002), iSBN 1-57331-371-8.

[9] Meier, R.; Merkle, K.; Maier, G.; Zarzalis, N.; Leuckel, W. and Wittig, S., *Proceedings of the 15th Annual Conference on Liquid atomization and spray systems, Toulouse, France, 5.-7. Juli.* (1999).

[10] Carvalho, I. S. and Heitor, M. V., *Experiments in Fluids*, 24:408–415 (1998).

[11] Braun, S.; L., W.; Koch, R. and H.-J., B., *Proceedings of the 10th International SPHERIC Workshop* (2015).

[12] Sauer, B.; Sadiki, A. and Janicka, J., *Journal of Computational Multiphase Flows*, 6(3):179–192 (2014).

[13] Eckel, G.; Rachner, M.; Clercq, P. L. and Aigner, M., *8th International Conference on Multiphase Flow, Jeju, Korea*, Jeju, Korea (2013).

[14] Gepperth, S.; Koch, R. and Bauer, H.-J., *ASME Turbo Expo 2013: Turbine Technical Conference and Exposition*, American Society of Mechanical Engineers (2013).

[15] Andreini, A.; Bianchini, C.; Caciolli, G.; Facchini, B.; Giusti, A. and Turrini, F., *Proceedings of ASME Turbo Expo 2014: Turbine Technical Conference and Exposition, Düsseldorf, Germany* (2014).

[16] Senecal, P.; Schmidt, D.; Nouar, I.; Rutland, C.; Reitz, R. and Corradini, M., *International Journal of Multiphase Flow*, 25(6-7):1073 – 1097 (1999).

[17] Chaussonnet, G.; Riber, E.; Vermorel, O.; Cuenot, B.; Gepperth, S. and Koch, R., *International Conference on Liquid Atomization and Spray Systems* (2013).
[18] Chaussonnet, G.; Vermorel, O.; Riber, E. and Cuenot, B., *International Journal of Multiphase Flow*, 80:29–42 (2016).
[19] Müller, A.; Meier, R.; Schäfer, O. and Wittig, S., *Atomization and Spray Processes* (2004).
[20] Gepperth, S.; Baerow, E.; Koch, R. and Bauer, H.-J., ILASS-Europe (2014).
[21] Bärow, E.; Gepperth, S.; Koch, R. and Bauer, H.-J., *Zeitschrift für Physikalische Chemie*, 229(6):909–929 (2015).
[22] Kapulla, R.; Tuchtenhagen, J.; Müller, A.; Dullenkopf, K. and Bauer, H.-J., *GALA Fachtagung Lasermethoden in der Strömungsmesstechnik* (2008).
[23] Müller, A., *Experimentelle Untersuchung des Zerstäubungsverhaltens luftgestützter Brennstoffdüsen bei oszillierenden Strömungen*, Ph.D. thesis, Institut für Thermische Strömungsmaschinen (ITS), Karlsruher Instituts für Technologie (KIT) (2015).
[24] Hecht, E., *Optics (4th Edition)*, Addison Wesley, 4th edn. (2001).
[25] Dauch, T.; Braun, S.; L., W.; Chaussonnet, G.; Keller, M.; Koch, R. and H.-J., B., *ASME 2016 Turbo Expo: Turbine Technical Conference and Exposition* (2016).
[26] Lefebvre and H., A., *Gas Turbine Combustion: Alternative Fuels and Emissions, Third Edition*, CRC Press (2012).